



Solar-Fenton catalytic degradation of phenolic compounds by impure bismuth ferrite nanoparticles synthesized via ultrasound



Tayyabe Soltani^a, Mohammad H. Entezari^{a,b,*}

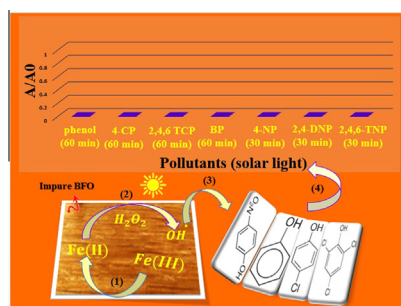
^a Sonochemical Research Center, Department of Chemistry, Ferdowsi University of Mashhad, 91775 Mashhad, Iran

^b Environmental Chemistry Research Center, Department of Chemistry, Ferdowsi University of Mashhad, 91775 Mashhad, Iran

HIGHLIGHTS

- Impure BFO as a heterogeneous catalyst was more effective than pure one.
- Complete degradation of phenolic compounds was achieved by the solar Fenton catalyst.
- Nitro derivatives in 30 min and others in 60 min were completely degraded.
- Hydroxyl radical exhibited a major role in degradation in dark and light.
- Surface active sites of the catalyst can be recovered in the cyclic mechanism.

GRAPHICAL ABSTRACT



ARTICLE INFO

Article history:

Received 22 December 2013

Received in revised form 3 March 2014

Accepted 8 April 2014

Available online 24 April 2014

Keywords:

Impure bismuth ferrite

Ultrasound

Phenolic compounds

Solar-Fenton catalyst

Solar light

ABSTRACT

In this work, a heterogeneous oxidation of phenolic compounds was examined by impure bismuth ferrite (BiFeO_3) nanoparticles synthesized by ultrasound. The nanoparticles were characterized by different techniques. The impure nanoparticles were more effective than pure one. The heterogeneous solar-Fenton catalytic degradation of phenolic compounds was used for the first time. A complete degradation of the phenolic compounds was achieved along with easy separation of the catalyst from the solution by an external magnetic field. The limitations of Fenton reaction such as iron sludge and slow regeneration of Fe(II) ions improved in this work. In the present work, a multivariate analysis has been used to assess the conditions for obtaining complete degradation in terms of the oxidant and catalyst concentrations. The response surface methodology (RSM) was performed to evaluate the effects of the two major factors (amount of impure BiFeO_3 magnetic nanoparticles (BFO MNPs) and concentration of H_2O_2) during the process. The effect of other variables such as initial concentration of phenol and initial pH was also examined. Partial oxidation of phenol took place at dark and a complete degradation was achieved at light in 60 min. The Fenton catalytic degradation mechanism was determined in dark and light. New reaction sites can be generated on the solid surface by the conversion of Fe(III) to Fe(II) for the generation of hydroxyl radical ($\text{OH}\cdot$). The effect of different electron acceptors on the heterogeneous solar-Fenton catalytic degradation of phenol was examined too. In addition, the solar-Fenton catalytic degradation of derivatives of phenol such as 4-chlorophenol (4-CP), 2,4,6-trichlorophenol (2,4,6-TCP), biphenyl (BP), 4-nitrophenol (4-NP), 2,4 dinitrophenol (2,4 DNP) and 2,4,6-trinitrophenol (2,4,6-TNP) was evaluated for the first time. Phenol and its derivatives completely degraded under solar light irradiation by the solar-Fenton catalyst in a short time with low concentration of H_2O_2 .

© 2014 Elsevier B.V. All rights reserved.

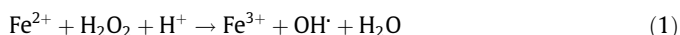
* Corresponding author at: Sonochemical Research Center, Department of Chemistry, Ferdowsi University of Mashhad, 91775 Mashhad, Iran. Fax: +98 511 8795457.

E-mail address: moh_entezari@yahoo.com (M.H. Entezari).

1. Introduction

Phenol and its derivatives widely used as raw materials in many industries. They are important pollutants in aquatic environment due to their toxicity, stability, carcinogenic and mutagenic potentials [1]. Recently, removal of phenols from industrial wastewater has generated considerable attention of the societies and attain to a safety level ($0.1\text{--}1.0\text{ mg L}^{-1}$) is difficult [2].

The advanced oxidation processes (AOPs), which can produce oxidizing hydroxyl radicals (OH^\cdot), have been proven to be an efficient method for the degradation of organic pollutants [3,4]. Among AOPs, Fenton-based processes (Eq. (1)) have been encountering a notable development due to their favorable results [5]. In this reaction, a mixture of H_2O_2 and Fe^{2+} in acidic solution generates the OH^\cdot [6].



The photo-Fenton reaction combines light, Fe^{3+} , and H_2O_2 . It can also facilitate the production of OH^\cdot by a photochemical route according Eq. (2) due to the decomposition of the photoactive $\text{Fe}(\text{OH})^{2+}$ species in mildly acidic solutions (pH 2.5–5) [7].



In these reactions, iron is cycled between the +2 and +3 oxidation states, so Fe^{2+} is not depleted and OH^\cdot production is limited only by the availability of light and H_2O_2 [8].

The Fenton reaction has high mineralization efficiency, inexpensive, easy in use, and environmental friendliness and also light irradiation can improve the production of OH^\cdot by photo Fenton reaction [9,10]. But, it has been reported that Fenton homogeneously catalyzed reactions requires concentrations of ca. $50\text{--}80\text{ mg L}^{-1}$ of iron ions in solution which is quite above the 2 ppm permitted by the European Community Directives [11]. Thus, in order to eliminate the iron ions from solution, precipitation and re-dissolution, other processes are essential with the additional operational costs. This limitation can be improved by development of dark- and photo-Fenton reactions based on heterogeneous catalytic systems that provide an easy separation and recovery of the catalyst from the solution [12,13]. Furthermore, unlike homogeneous Fenton reaction which requires a strict control of pH around 2–3 for an excellent catalytic performance, immobilized Fenton catalytic systems provide the possibility of working in a wider pH range. The critical point of these reactions is the stability of immobilized iron species to be leached out into the solution under the typically acidic and strong oxidizing conditions in which Fenton reactions occur. Today, many efforts are currently performed to design new photocatalysts with high resistance and allowing an efficient use of the OH^\cdot due to the relative high cost of H_2O_2 .

Nanosized iron oxides exhibit high catalytic activity because of their large surface area, which potentially provides more active sites for the generation of OH^\cdot [14–16]. Furthermore, bismuth ferrite (BiFeO_3) with a rhombohedrally distorted perovskite structure is a new important visible-light photocatalyst for the degradation of organic pollutants because of its narrowing band gap energy (2.2 eV) and excellent chemical stability [17–19]. This photocatalyst is completely different than photocatalysts such as CdS which suffers from instability against the photo irradiation [20]. It was found that BiFeO_3 magnetic nanoparticles (BFO MNPs) effectively catalyzed the decomposition of H_2O_2 into OH^\cdot , being confirmed with electron spin resonance spin-trapping technique and other probing techniques. The synthesis of BFO MNPs by various methods often is complex and performs at high temperature ($800\text{ }^\circ\text{C}$) which lead to impurity phases such as Bi_2O_3 , Fe_2O_3 , $\text{Bi}_{25}\text{FeO}_4$, $\text{Bi}_2\text{Fe}_4\text{O}_9$ and $\text{Bi}_{36}\text{Fe}_{24}\text{O}_{57}$ [21–23].

Ultrasound was found to be more efficient for fabrication and modification of nanosized materials because of acoustic cavitation which is the formation, growth and collapse of the bubbles in liquid [24,25]. Sono-synthesis of BFO MNPs with high photocatalytic activity in degradation of various azo dyes under solar light irradiation was investigated in our lab [26–28]. Nanoparticles synthesized with ultrasound had smaller crystallite size and higher photocatalytic activity than the nanoparticles synthesized with classical method [27].

The main purpose of this work is the assessment of impure BFO MNPs as a new nanocomposite for the heterogeneous Fenton and solar-Fenton catalytic degradation of phenolic compounds from aqueous solutions. High energetic 254 nm UV radiation and UV near visible irradiation ($>313\text{ nm}$) used by some authors [29–31] has been replaced by solar light in this study, which represents a significant advantage for the future application.

2. Experimental

2.1. Chemical and materials

Bismuth nitrate ($\text{Bi}(\text{NO}_3)_3 \cdot 5\text{H}_2\text{O}$), iron nitrate ($\text{Fe}(\text{NO}_3)_3 \cdot 9\text{H}_2\text{O}$) and ethylene glycol (EG) from Merck have been used without further purification for the synthesis of impure BFO. Phenol and its derivatives include 4-chlorophenol (4-CP), 2,4,6-trichlorophenol (2,4,6-TCP), biphenyl (BP), 4-nitrophenol (4-NP), 2,4 dinitrophenol (2,4 DNP) and 2,4,6-trinitrophenol (2,4,6-TNP) from Merck were used as pollutants. H_2O_2 was purchased from Fluka. Ethanol, isopropanol (IP) were analytical reagent grade and used without further purification. Sodium persulfate ($\text{Na}_2\text{S}_2\text{O}_8$) and potassium bromate (KBrO_3) were used as electron acceptors from Merck.

2.2. Preparation of impure BFO MNPs

In a typical procedure, 0.008 mol $\text{Bi}(\text{NO}_3)_3 \cdot 5\text{H}_2\text{O}$ was sonicated in EG for 15 min. After ultrasonic dispersion, a transparent solution was formed and the temperature of solution was increased from 9 to $35\text{ }^\circ\text{C}$. The stoichiometric amount of $\text{Fe}(\text{NO}_3)_3 \cdot 9\text{H}_2\text{O}$ was added into the solution and the mixture was sonicated for another 5 min to obtain a brownish red sol at the same temperature. The sample dried at $70\text{ }^\circ\text{C}$ and a xerogel powder was formed. Consequently, the remained powder was maintained at $400\text{ }^\circ\text{C}$ for 0.5 h. Finally, the as-prepared sample washed with distilled water and absolute alcohol for several times and dried at $70\text{ }^\circ\text{C}$.

2.3. Characterization and equipment

The crystalline structure was identified by X-ray diffraction (XRD, Philips PW1800) employing $\text{Cu K}\alpha$ ($\lambda = 1.5406\text{ \AA}$, $2\theta = 10\text{--}70^\circ$). The magnetization of the nanoparticles was measured with vibrating sample magnetometer (VSM, HH-20) operating at ambient temperatures. The light absorption ability of the sample was analyzed by UV–vis diffuse reflectance spectra (DRS, MC-2530). The absorption spectrum of phenol and its derivatives were measured using a UV–vis spectrophotometer (Unico 2800). Atomic absorption spectrophotometer (AAS, Varian, spectra-110 880/220-Australia Pty Ltd.) was used to determine the concentration of the Fe and Bi ions in the solution during the phenol degradation.

The ultrasonic irradiation was applied with equipment operating at 20 kHz (Branson Digital sonifier, W-450 D).

2.4. Activity test

The catalytic activity of impure BFO MNPs has been evaluated in a heterogeneous dark Fenton and photo Fenton catalytic

degradation of phenol and its derivatives from aqueous solution. In this case, several Erlenmeyer flask containing 100 mL phenol (50 mg L^{-1}), $0.8 \text{ mM H}_2\text{O}_2$ and 0.06 g of catalyst at $\text{pH } 2.5$ were magnetically stirred in a dark place for 15 min. Then, the solutions were perched on the shaker with mixing rate of 400 rpm for different interval times under direct solar light radiation in consecutive sunny days in May 2013 between 10 am and 3 pm (GPS coordinates: $N = 36^\circ 18' 41.6''$, $E = 59^\circ 31' 54.2''$). The temperature of the solution was kept between 28 and 32°C . At given interval times, about 5 mL of suspensions sampled and separated from the solution with an external magnetic field. The mentioned conditions were fixed for all experiments. The removal efficiency of phenol was determined based on the absorption at 270 nm by UV–vis spectrophotometer.

The removal efficiency (R (%)) was defined by the following expression:

$$(R \text{ (%)}) = \left(1 - \frac{A}{A_0}\right) \times 100 \quad (3)$$

In this equation, A_0 and A are the absorbance of phenol aqueous solution at time 0 and t at $\lambda_{\text{max}} = 270 \text{ nm}$, respectively.

Experiments under different pH were also performed to reveal the role of pH on the photocatalytic activity of impure BFO MNPs. The pH values were adjusted by adding HCl or NaOH.

3. Results and discussion

3.1. Characterization of the catalyst

The sono synthesis of pure BFO MNPs at calcination temperatures of 400°C for 0.5 h and 500°C for another 0.5 h has been reported in our recent work [27]. All the reflection peaks was readily indexed to the pure rhombohedral structure of BFO MNPs (Space group: $R3c$) with lattice parameters of $a = b = 5.576 \text{ \AA}$ and $c = 13.867 \text{ \AA}$, which were in good agreement with the literature data (JCPDS 86-1518).

Based on the $\text{Bi}_2\text{O}_3\text{--Fe}_2\text{O}_3$ phase diagram, BFO MNPs is incongruently melting compound [32] and kinetics of phase formation in the $\text{Bi}_2\text{O}_3\text{--Fe}_2\text{O}_3$ system can easily lead to the appearance of impurities such as $\text{Bi}_{25}\text{FeO}_{40}$ and $\text{Bi}_2\text{Fe}_4\text{O}_9$ [33]. Furthermore, slowing down the heating rate and slow quenching to room temperature will lead to the some impurities that might be ascribed to the decomposition of BFO during the slowly heating rate process [32].

As shown in Fig. 1, slowing down the heating rate and slow quenching to room temperature when the sample was calcined only at 400°C for 0.5 h, led to other phases such as Bi_2O_3 and Fe_2O_3 in the diffraction patterns of BFO MNPs. These impurities indicate partially reactions occurred at this calcination temperature. The sample obtained was brown–red in color and proportions of BFO MNPs, Bi_2O_3 and Fe_2O_3 were 64%, 15% and 21%, respectively and the cell parameters for impure BFO MNPs with space group $R3c$ were bigger than pure one ($a = b = 5.589$ and $c = 13.894$). These lattice parameters were in reasonable agreement with those reported in the literature (JCPDS 86-1518). The average crystallite size obtained from the Debye–Scherrer formula for the impure BFO MNPs was 32.86 nm .

The magnetic properties of the impure BFO MNPs were measured by VSM at room temperature. Fig. 2 shows the variation of magnetization (M) versus applied field (H). As shown in Fig. 2, an obvious ferromagnetism (FM) property can be found with a magnetic saturation of about 13.0 emu g^{-1} at 300 K . A comparison between pure and impure BFO MNPs shows that impure nanoparticles exhibited higher magnetization than pure nanoparticles (3.0 emu g^{-1}) [27]. This behavior can be related to the other

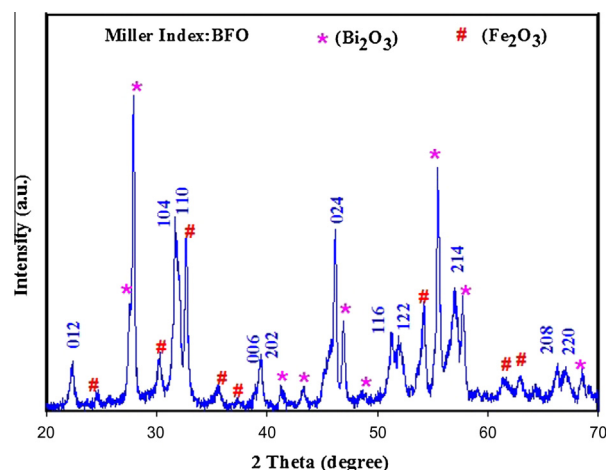


Fig. 1. XRD pattern of impure BFO MNPs synthesized via ultrasound.

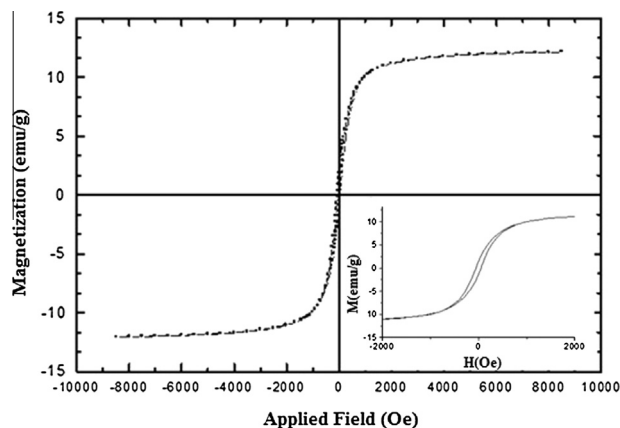


Fig. 2. Magnetic hysteresis loops at room temperature.

impurities such as Fe_2O_3 and the smaller crystallite size of nanoparticles [34].

3.2. UV–vis analysis

The optical absorption of the impure BFO MNPs synthesized via ultrasound is presented in Fig. 3. The absorption spectrum shows a strong photo absorption in the visible light region. The inset of Fig. 3 shows the optical band gap energy of the nanoparticles by using Tauc's equation [35], and the calculated value is 2.2 eV which is quite comparable with our previous reports [27]. Thus, the synthesized nanoparticles have a potential application as an appropriate catalyst for degradation of the pollutants in the visible region.

3.3. Decomposition of phenol in dark and light

3.3.1. Pure and Impure

Two types of heterogeneous Fenton and solar-Fenton catalytic degradation of phenol were compared with pure and impure MNPs. At first, the solutions were magnetically stirred in a dark place to attain maximum degradation and then, the experiments were carried out under different times of solar light irradiation. The results show that the impure BFO MNPs were more efficient than pure one. The high activity of impure BFO MNPs can be attributed to the solar-Fenton reactions and photocatalytic reactions occurring on the BFO MNPs and other oxides present in the impure

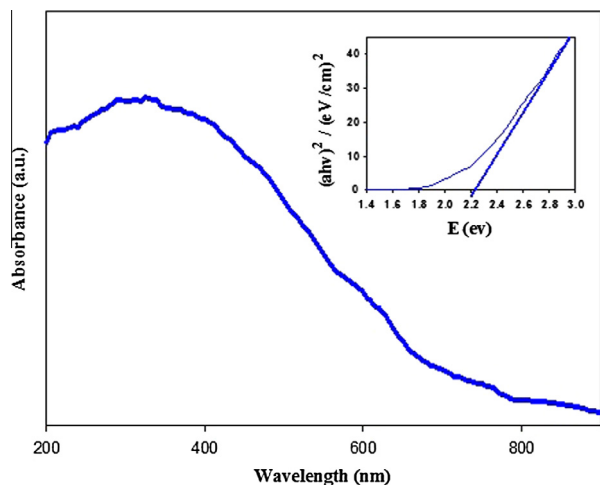


Fig. 3. UV-vis DRS spectrum of impure BFO MNPs, the inset shows the band gap energy.

one. In particular, the synergistic photocatalytic activity between the three components can accelerate the formation of Fe(II) site in light.

Furthermore, other experiments on the heterogeneous photo-Fenton catalytic degradation of organic pollutants demonstrated that polymer films contain titanium oxide and iron oxide had synergistic photocatalytic activity at neutral pH [36,37]. Iron oxides with two or more components exhibit unique chemical and physical properties. Chemically, the combination of two oxides exerts a synergistic effect that outweighs the sum of the effects of all individual components [38].

As the impure BFO MNPs with a synergistic effect of two or more oxides were more efficient than pure one, therefore, the whole experiments were performed with the impure BFO MNPs.

3.3.2. Phenol and H₂O₂ or phenol and catalyst

When the solution of phenol in the presence of H₂O₂ or impure BFO MNPs was irradiated by solar light for 60 min, in both cases, no degradation of phenol was observed (Tables 1 and 2). Therefore, phenol cannot be degraded directly by solar light in the presence of H₂O₂ or impure BFO MNPs, separately. On the other hand, the photolysis (alone or combined with an oxidant, such as H₂O₂) and photo catalysis with impure BFO cannot be effective for degradation of phenol.

3.3.3. Phenol, catalyst, and H₂O₂

3.3.3.1. Catalyst and H₂O₂ concentration. The optimum catalyst loading and H₂O₂ concentration are important parameter to ensure the minimum use of them. Therefore, the removal efficiency of phenol was examined in dark and solar light with different doses of catalyst and H₂O₂ concentrations at initial pH of 2.5. At first, one variable was kept constant and the other was varied within the experimental ranges (Tables 1 and 2). Second, two variables changed with each other (Fig. 4).

As summarized in Tables 1 and 2, the removal efficiency of phenol proceeded slowly in the dark place when one of the variables (doses of catalyst or H₂O₂ concentration) was constant and another

one was varied during the process. The results show that only 13% of phenol was degraded when the initial H₂O₂ concentration was fixed at 0.7 mM and the catalyst loading increased from 0.01 to 0.07 g. Similarly, 12% of phenol was degraded by increasing the H₂O₂ concentration from 0.02 to 1.0 mM with constant dosage of the catalyst at 0.05 g. In the presence of solar light irradiation, the extent of degradation efficiency of phenol was strongly improved with increasing the catalyst loading or H₂O₂ concentration. By increasing the catalyst dosage and H₂O₂ concentration, the amount of H₂O₂ decomposition was increased and produced more OH[•] for the degradation of phenol molecules. The higher activity with light is attributed to the combination of nanophotocatalysis and solar-Fenton-catalysis processes on the impure BFO MNPs and other oxides.

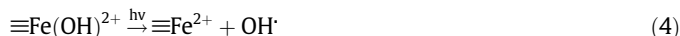
Complete removal efficiency was obtained when the values of each operational parameter were justified at the optimum values. The response surface methodology (RSM) was developed as a function of the H₂O₂ concentration and catalyst dosage while time of irradiation was kept constant. This experimental design methodology was carried out for impure BFO catalyst loadings (0.01–0.08 g) and H₂O₂ concentrations (0.02–1.12 mM) at first in dark and then in the presence of solar light as shown in Fig. 4a and b.

In dark place, partial degradation of phenol was improved by simultaneous increasing of H₂O₂ concentration and catalyst dosage (Fig. 4a). In the presence of solar light, phenol removal efficiency increased quickly with increasing both variables and a complete degradation of phenol was obtained using 0.06 g impure BFO MNPs and 0.8 mM H₂O₂ (Fig. 4b). The higher concentrations of H₂O₂ and catalyst from optimized values have led to a decrease in catalytic performance.

The optimized value of catalyst (0.06) and H₂O₂ concentration (0.8 mM) were used for other experiments.

3.3.3.2. pH of medium. The pH of the medium is another important parameter. It directly affects not only the photo-catalytic performance, but also affects the OH[•] concentration in heterogeneous solar-Fenton catalytic processes [39]. As shown in Fig. 5, under natural and basic media, the solar-Fenton catalytic efficiency over impure BFO MNPs can be ignored. But with decreasing the pH from 5.5 to 2.5, the degradation efficiency greatly increased. Fig. 5 shows that the maximum solar-Fenton catalytic degradation obtained at pH = 2.5 without any change in the initial pH.

At acidic pH, the predominant iron sites is ≡Fe(H₂O)₅(OH)²⁺ [or simply ≡Fe(OH)²⁺] which can absorbs solar light. Studies of the photochemistry of ≡Fe(OH)²⁺ have shown that this species undergoes a relatively efficient photoreaction to produce ≡Fe(II) and the OH[•] (Eq. (4)) [7].



In this case, solar-Fenton catalytic process not only forms ≡Fe(II), the major catalytic species in the Fenton catalytic reactions, but also produces an additional OH[•] which is responsible for the degradation of organic material [7].

Under alkaline conditions, a high-valence iron species (≡Fe(IV)=O, Eq. (5)) may be formed during the reaction [39,40]. It was confirmed that ≡Fe(IV)=O species are less reactive than OH[•] and cannot react with aromatic compounds [39].

Table 1
Effect of amount of catalyst on the Fenton catalytic degradation of phenol.

Catalyst (g)	0.0	0.01	0.02	0.03	0.04	0.05	0.06	0.07
Removal (%) (dark)	No degradation	3.5	4.9	5.7	6.6	8.9	12.2	13.3
Removal (%) (solar light)	No degradation	17.1	30.5	49.5	69.7	80.2	91.3	97.3

Table 2
Effect of concentration of H₂O₂ on the Fenton catalytic degradation of phenol.

H ₂ O ₂ (mM)	0.0	0.02	0.1	0.3	0.6	0.7	0.8	1.0
Removal (%) (dark)	No degradation	3.2	4.4	5.1	5.4	7.2	11.1	12.1
Removal (%) (solar light)	No degradation	13.2	25.2	36.2	55.2	72.3	86.3	95.2

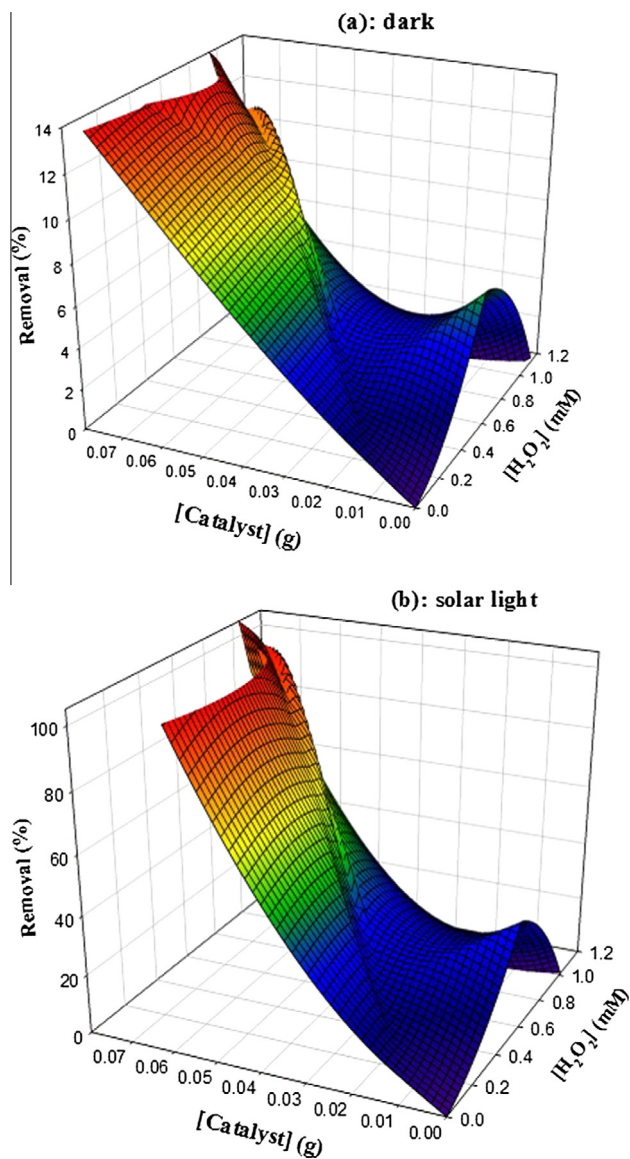
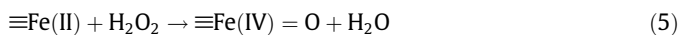


Fig. 4. 3D response surfaces of removal efficiency (a): dark and (b) solar light (temp., 30 °C, initial pH = 2.5).



In these equation, \equiv represent the sites on the solid surface of the impure BFO MNPs.

3.3.3.3. Initial concentration. The effect of initial concentration of phenol was studied in the range of 40–100 mg L⁻¹ in 60 min of irradiation. As shown in Fig. 6, the solar-Fenton catalytic degradation of phenol was only completed at 50 mg L⁻¹ and the degradation was reduced at higher and lower concentrations.

As shown in Fig. 6, solar Fenton catalytic degradation of phenol was reduced to 46% with 25 mg L⁻¹ catalyst. The oxidation of phenol was mostly carried out by the OH[•] produced from the reaction

between H₂O₂ and $\equiv\text{Fe(II)}$. Therefore, the optimum concentration of the reactants is necessary. In this case, the concentrations of H₂O₂ and $\equiv\text{Fe(II)}$ are in excess compared to the phenol molecules. Therefore, the OH[•] can produce H₂O₂ with reaction by itself or can be trapped as expressed by the following equations [41–43].



On the other hand, when the initial phenol concentration increased from 50 mg L⁻¹, the removal efficiency decreased. The decrease in degradation rate at higher concentrations is attributed to the phenol molecules in solution which are more than OH[•] and $\equiv\text{Fe(II)}$ species.

3.4. Solar-Fenton catalytic degradation under optimum conditions

3.4.1. UV–vis spectroscopy

UV–vis absorbance spectra of phenol during solar-Fenton catalytic degradation are shown in Fig. 7. The spectrum contains two absorption bands centered at 270 and 225 nm, corresponding to $n \rightarrow \pi^*$ and $\pi \rightarrow \pi^*$ transitions. First, the phenol solution was stirred at dark from 15 to 120 min and similar partial degradation of phenol was obtained in this range of time (Fig. 7). The Fenton catalytic results showed the disappearance of phenol peaks after 15 min. The color of the solution changed from colorless to yellowish after this time. These behaviors can be related to the formation of polycarboxylic acid intermediates with opening the aromatic rings in dark [44,45]. Then, the solution was placed under solar light irradiation for different interval times. By increasing the irradiation time, the absorption peaks gradually reduced and finally vanished within 60 min. Furthermore, the color of the solution changed from yellowish to colorless after 60 min at light.

This behavior is consistent with the fast destruction of phenol molecules. In the presence of solar light irradiation, the intermediates formed in dark can be degraded. The high TOC decay confirms that the photo Fenton catalytic degradation can effectively degrade the phenol molecules to CO₂ and H₂O.

3.5. Possible degradation mechanism

3.5.1. In dark

The results show that H₂O₂ in dark by contact with Fe(III) sites available on the surface of impure BFO MNPs can initiate chain reactions that leads to the formation of OH[•]. Under acidic medium, the mechanism of the H₂O₂ activation by impure BFO MNPs may involve the following Eqs. ((9)–(14)). At first, a complex between $\equiv\text{Fe(III)}$ and H₂O₂ being assigned as $\equiv\text{Fe(III)H}_2\text{O}_2$ is generated on the surface of impure BFO MNPs (Eq. (9)). The generated species ($\equiv\text{Fe(III)H}_2\text{O}_2$) are converted to $\equiv\text{Fe(II)}$ and HO₂ species (Eq. (10)). Furthermore, $\equiv\text{Fe(II)}$ species can be generated on the surface of impure BFO MNPs by reaction of generated HO₂ with $\equiv\text{Fe(III)}$ (Eq. (11)). All of the formed $\equiv\text{Fe(II)}$ species on the surface of impure BFO MNPs can be reacted with H₂O₂ to produce OH[•] (Eqs. (12) and (13)). Then, the generated OH[•] attack to the phenol molecules for partial degradation in dark (Eq. (14)). This mechanism is

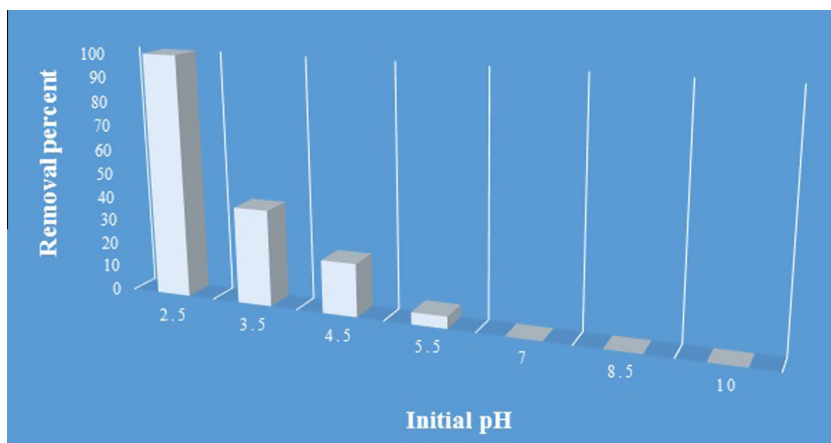


Fig. 5. Effect of initial pH on the solar Fenton catalytic degradation of phenol, (temp., 30 °C, concentration of H₂O₂ = 0.8 mM, dose of catalyst = 0.06 g, time of irradiation = 60 min).

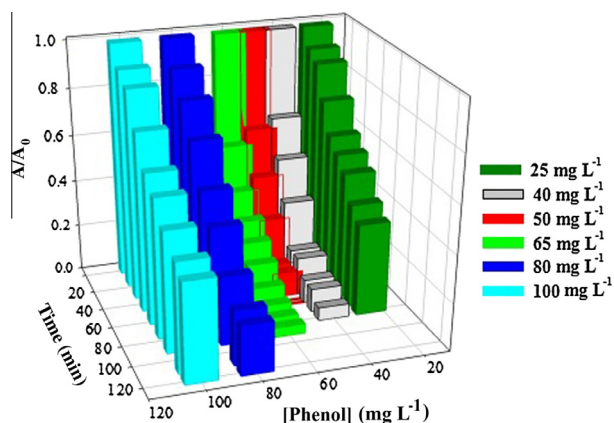


Fig. 6. Effect of initial concentration of phenol on the solar Fenton catalytic degradation of phenol, (temp., 30 °C, concentration of H₂O₂ = 0.8 mM, dose of catalyst = 0.06 g, initial pH = 2.5).

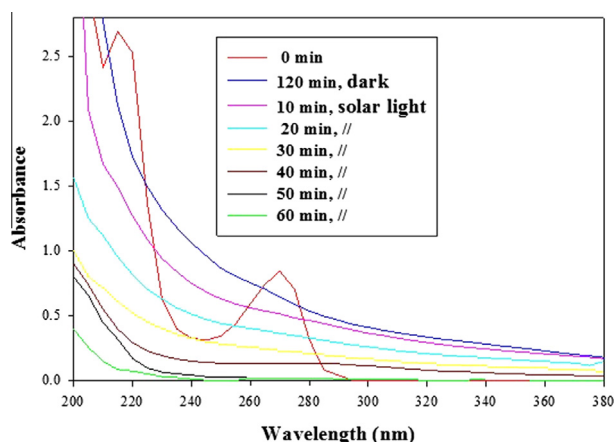
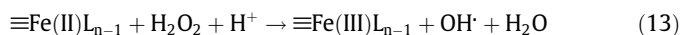
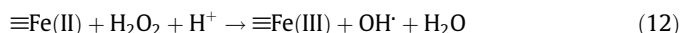
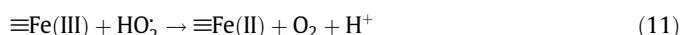
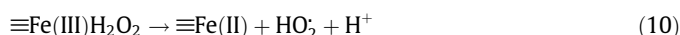
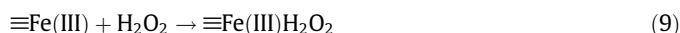


Fig. 7. UV-vis absorption spectra of phenol solution at different time of irradiations at dark and solar light, (temp., 30 °C, concentration of H₂O₂ = 0.8 mM, dose of catalyst = 0.06 g, initial pH = 2.5).

in accordance with the results in the literature [46–48], which iron oxide could activate H₂O₂ to produce OH[•]. This mechanism confirmed with electron spin resonance, spin-trapping and other techniques too.

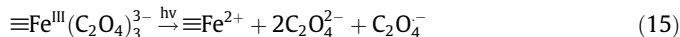


The result demonstrates the restricted production of OH[•] by catalytic dark-Fenton reactions at these particular conditions. Other results confirmed that the formation of polycarboxylic acid intermediates with opening the aromatic rings in dark [44,45].

In Eq. (13), L shows complexing agent or polycarboxylic acid which linked to the surface of the catalyst.

3.5.2. In light

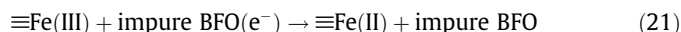
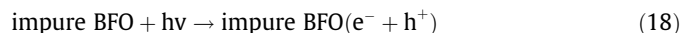
In this case, the yield of ≡Fe(II) greatly increases when ≡Fe(III) is complexed with carboxylic anion such as oxalate [44,45] formed in dark as an intermediate. The ferrioxalate complex Fe^{III}(C₂O₄)₃³⁻ is highly photosensitive and is used as the basis of well known chemical actinometer at acidic pH [49]. The reduction of ≡Fe(III) to ≡Fe(II), through a photoinduced ligand to metal charge transfer, can occur over the ultraviolet and into the visible region according to the reactions of (15)–(17) [50].



In the presence of solar light irradiations, another possible mechanism can be written in the form of the following Eqs. (18)–(23) [38]. This mechanism is a combination of solar-Fenton catalytic reactions and photocatalytic reactions on the surface of impure BFO MNPs. New reaction sites can be formed on the surface of impure BFO MNPs by the photo-reduction of ≡Fe(III) to ≡Fe(II).

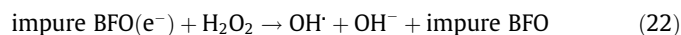
The impure BFO is a narrow band gap photocatalyst. When it is illuminated with solar light, electrons are promoted from the valence band to the conduction band to give electron-hole pairs through reaction (18). Then, the dissolved oxygen can act as a photogenerated electron scavenger to give O₂^{-•} (19). The next

reaction is a simple redox reaction in which O_2^- is oxidized to O_2 and $\equiv Fe(III)$ is reduced to $\equiv Fe(II)$ (20). Finally, the photo-reduction of $Fe(III)$ takes place on the surface of impure BFO MNPs to $Fe(II)$ under irradiation of solar light according to Eq. (21).



The impure BFO MNPs with two or more components exhibited more photocatalytic activity than pure one. The higher activity is attributed to the solar catalytic reactions occurring on the BFO MNPs and other oxides (reactions (18)–(21)). In addition, the combination of three oxides reduce electron-hole pair recombination (reaction (18)). On the other hand, combination of oxides exerts a synergistic effect that outweighs the sum of the effects of all individual components. Finally, the synergistic photocatalytic activity between the three oxides can accelerate $\equiv Fe(II)$ and OH^\cdot generation under the light [36–38].

Furthermore, H_2O_2 can act as an electron acceptor to increase the OH^\cdot concentration as given by the following reactions:



Then, the whole $\equiv Fe(II)$ species formed on the surface of the solid can activate H_2O_2 with solar-Fenton catalytic mechanism to produce additional OH^\cdot in the solution, while themselves are oxidized into $\equiv Fe(III)$ (Eqs. (12) and (13)). Finally, the new generated OH^\cdot species can mineralize the carboxylic anion intermediates which produced in dark place to CO_2 and H_2O .

3.5.3. Confirming the mechanism

Some experiments were designed to prove the proposed mechanism of degradation. The effect of impure BFO MNPs in production of $\equiv Fe(II)$ active species was studied by two separate experiments in the presence and absence of quencher under identical conditions (Fig. 8). After addition of IP (20 mM) as a scavenger of OH^\cdot [51,52], the degradation of phenol was completely inhibited even at dark. This implies that OH^\cdot play a major role in the degradation of phenol. The predominant oxidation route of IP ($RCHOHR$, $R=CH_3$) involves α -hydrogen abstraction and generating the

$RCOHR$ radical (Eq. (24)) [44]. In this case, the OH^\cdot produced in dark and light react with IP and the degradation of phenol molecules was completely inhibited according to the following reaction:



The results show similar behaviors at higher and lower dosage of 0.06 g. Because in these cases, the total OH^\cdot produced in medium trap with IP too. It was also reported that at lower concentrations of IP, the following scavenging reactions become competitive:



The symbol $HC_2O_4^-$ in reaction (26) is used to represent all of the formed oxalate in dark. It is assumed that OH^\cdot can still attack oxalate anions when it is coordinated with $\equiv Fe(III)$ in low concentration of IP [44].

To understand the effect of oxygen, one experiment was conducted without O_2 . In this case the result show that, the solar-Fenton catalytic degradation of phenol was prohibited strongly under Ar atmosphere, which means that O_2 has a major role in solar-Fenton catalytic decomposition too (Fig. 8). Ferrous iron on the impure BFO MNPs surface reacts with oxygen through a series of one-electron transfer to produce hydrogen peroxide (Eqs. (27) and (28)). Then, H_2O_2 ultimately reacts with ferrous iron on the surface of impure BFO MNPs via the Fenton catalytic reaction to produce an oxidizing intermediate of OH^\cdot (Eqs. (12) and (13)), which then reacts with the contaminant and led to the complete mineralization [44].



Also, in the lack of O_2 molecules, the other reactions for the generation of OH^\cdot was also prohibited (Eqs. (19), (20), and (23)).

The results proved that, OH^\cdot and O_2 molecules are important species in the solar-Fenton catalytic degradation of phenol on the solid surface of impure BFO MNPs.

Furthermore, the catalytic mechanism of BFO MNPs was investigated with Monte Carlo (MC) simulation and density functional theory (DFT) calculations [53]. The MC simulations show that the H_2O_2 molecule tends to adsorb at the hollow site of BFO facets constitute of four Fe atoms. The H_2O_2 lies on the surface of BFO MNPs facets with O–O bond parallel to the surface. In addition, DFT calculations confirmed that the H_2O_2 adsorption is a chemical adsorption process. Furthermore, the DFT geometry optimization results showed that the O–O bond was elongated at the hollow sites with Fe atoms interaction and thereby the O–O bond was significantly weakened, corresponding to the generation of OH^\cdot at the hollow sites. This result coupled with the results of the fluorescence probing technique and ESR results [53].

The results of some electron scavengers such as $Na_2S_2O_8$ and $KBrO_3$ are summarized in Table 3. In the presence of these species (0.005 g L^{-1}), the solar-Fenton catalytic degradation of phenol was reduced in the presence of $S_2O_8^{2-}$, but, it was increased with addition of the BrO_3^- ions after 45 min of irradiation. The enhancement of solar-Fenton catalytic degradation of phenol in the presence of BrO_3^- could be attributed to the formation of the BrO_3^\cdot , which is very strong oxidizing species (Eq. (29)) [54]:



But, in the case of $S_2O_8^{2-}$, the $SO_4^{\cdot-}$ was formed which is less reactive than OH^\cdot (Eq. (30)) [55].

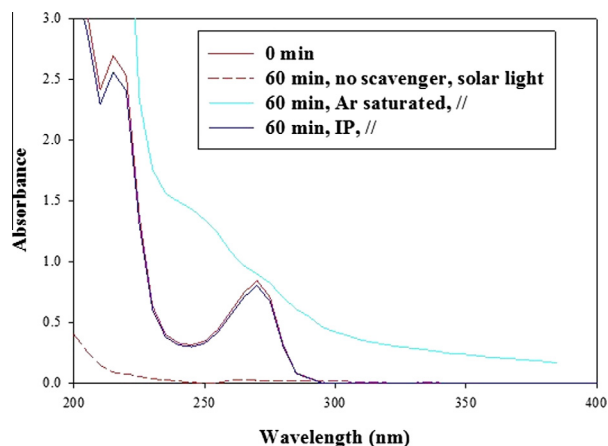


Fig. 8. UV-vis absorption spectra of phenol in the presence of different quenchers under solar light, (temp., 30 °C, concentration of $H_2O_2 = 0.8 \text{ mM}$, dose of catalyst = 0.06 g, initial pH = 2.5, time of irradiation = 60 min).

Table 3
Effect of different electron acceptors on the solar Fenton catalytic degradation of phenol.

Electron acceptor	H ₂ O ₂	Na ₂ S ₂ O ₈ + H ₂ O ₂	KBrO ₃ + H ₂ O ₂	Na ₂ S ₂ O ₈	KBrO ₃
Removal (%)	91.2	78.3	100.0	No degradation	No degradation

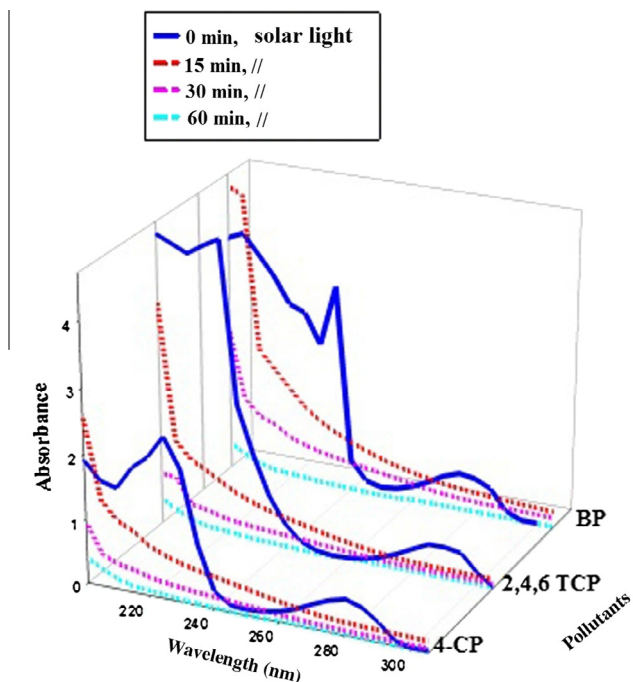


Fig. 9. UV-vis absorption spectra of CP derivatives and BP under solar light, (temp., 30 °C, concentration of H₂O₂ = 0.8 mM, dose of catalyst = 0.06 g, initial pH = 2.5).

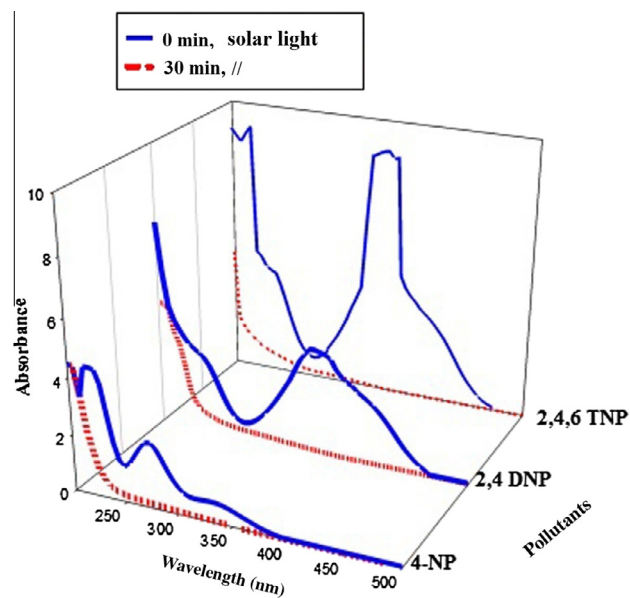
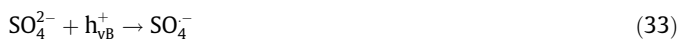


Fig. 10. UV-vis absorption spectra of NP derivatives under solar light, (temp., 30 °C, concentration of H₂O₂ = 0.8 mM, dose of catalyst = 0.06 g, initial pH = 2.5).

Furthermore, the SO₄^{•-} may also react with water molecule and photo-generated electron to produce more sulfate ions as follows:



In addition, the SO₄²⁻ can react with hole and OH[•] to produce SO₄^{•-}.



It should be mentioned that when S₂O₈²⁻ and BrO₃⁻ without H₂O₂ were used, the photo Fenton catalytic degradation of phenol was completely stopped (Table 3).

3.6. Stability and reusability of the BFO MNPs

The results show that impure BFO MNPs were stable and active under visible light irradiation during the photocatalytic degradation process. No leaching of Fe and Bi ions from impure BFO MNPs was detected during the phenol degradation at pH = 2.5 by AAS. The high chemical stability of impure BFO MNPs was further confirmed by FT-IR measurements on the catalyst before and after the phenol degradation too (not shown). The FT-IR results show that the surface of the used catalyst was the same as that of the fresh one.

3.7. Degradation of some derivatives of phenol

The solar-Fenton catalytic degradation was tested with some derivatives of phenol such as 4-CP, 2,4,6-TCP, BP, 4-NP, 2,4 DNP and 2,4,6-TNP. At first, the removal of phenolic compounds was examined in the dark for 15 min. The dark Fenton catalytic degradation of phenolic compounds can be preceded by cleavage of benzene rings to produce polycarboxylic acid intermediates. Then, the solutions were irradiated by solar light and the results are presented in Figs. 9 and 10. The absorption peaks of phenolic compounds were decreased in intensity by increasing the irradiation times and were completely vanished in relatively short time. The results show a complete degradation for nitro derivatives of phenol in 30 min, while for other derivatives longer times were required. The shorter time of degradation in nitro derivatives might be attributed to the adsorption of visible light for the excitation.

4. Conclusion

In this work, an impure BFO MNPs as a novel stable nanocomposite with a FM order and small crystallite size was prepared successfully by ultrasound. For the first time, the solar light was used in the heterogeneous photo-Fenton catalytic degradation of phenolic compounds for overcoming the limitation of the Fenton reaction in water treatment applications. The impure BFO MNPs with small crystallite size provide more active sites for the generation of OH[•] than pure one. The degradation of phenol and its derivatives were carried out through the dark and solar-Fenton catalytic approach. Partial degradation in dark and a complete degradation of phenolic compounds was obtained under solar light irradiation with 0.06 g of impure BFO MNPs and low concentration of H₂O₂ (0.8 mM). The synthesized magnetic nanoparticles can be effectively separated with an external magnetic field without any formation of the secondary metal ion pollutants during the process. The complete solar Fenton catalytic degradation of nitro derivatives was achieved in 30 min, while for other derivatives longer times were required.

The OH[•] and O₂ molecules were important species in the solar-Fenton catalytic degradation of the selected pollutants. The strong H₂O₂-activating ability of impure BFO MNPs showed promising applications in the oxidative degradation of organic pollutants.

Acknowledgement

The support of Ferdowsi University of Mashhad (Research and Technology) for this work (code 3/19022, date 2011/10/19) is appreciated.

References

- [1] V. Androulaki, A. Hiskia, D. Dimotikali, C. Minero, P. Calza, E. Pelizzetti, E. Papaconstantinou, Light induced elimination of mono and polychlorinated phenols from aqueous solutions by PW₁₂O₄₀, the case of 2,4,6-trichlorophenol, *Environ. Sci. Technol.* 34 (2000) 2024–2028.
- [2] N. Takahashi, T. Nakai, Y. Satoh, Y. Katoh, Variation of biodegradability of nitrogenous organic compounds by ozonation, *Water Res.* 28 (1994) 1563–1570.
- [3] P.R. Gogate, A.B. Pandit, A review of imperative technologies for wastewater treatment I: oxidation technologies at ambient conditions, *Adv. Environ. Res.* 8 (2004) 501–552.
- [4] P.R. Gogate, A.B. Pandit, A review of imperative technologies for wastewater treatment II: hybrid methods, *Adv. Environ. Res.* 8 (2004) 553–597.
- [5] J. Feng, X. Hu, P.L. Yue, S. Qiao, Photo Fenton degradation of high concentration orange II (2 mM) using catalysts containing Fe: a comparative study, *Sep. Purif. Technol.* 67 (2009) 213–217.
- [6] C. Walling, A. Goosen, Mechanism of the ferric ion catalyzed decomposition of hydrogen peroxide. Effect of organic substrates, *J. Am. Chem. Soc.* 95 (1973) 2987–2991.
- [7] V. Nadtochenko, J. Kiwi, Photolysis of FeOH²⁺ and FeCl²⁺ in aqueous solution. Photodissociation kinetics and quantum yields, *Inorg. Chem.* 37 (1998) 5233–5238.
- [8] J. Bacardit, J. Stotzner, E. Chamarro, S. Esplugas, Effect of salinity on the photo-Fenton process, *Ind. Eng. Chem. Res.* 46 (2007) 7615–7619.
- [9] A. Georgi, A. Schierz, U. Trommler, C.P. Horwitz, T.J. Collins, F.D. Kopinke, Humic acid modified Fenton reagent for enhancement of the working pH range, *Appl. Catal. B: Environ.* 72 (2007) 26–36.
- [10] M.M. Cheng, W.H. Ma, J. Li, Y.P. Huang, J.C. Zhao, Visible-light-assisted degradation of dye pollutants over Fe(III)-loaded resin in the presence of H₂O₂ at neutral pH values, *Environ. Sci. Technol.* 38 (2004) 1569–1575.
- [11] F. Martínez, G. Calleja, J.A. Melero, R. Molina, Heterogeneous photo-Fenton degradation of phenolic aqueous solutions over iron-containing SBA-15 catalyst, *Appl. Catal. B: Environ.* 60 (2005) 181–190.
- [12] H. Zhang, H.J. Choi, C.-P. Huang, Optimization of Fenton process for the treatment of landfill leachate, *J. Hazard. Mater.* 125 (2005) 166–174.
- [13] A.M.T. Silva, E. Nouli, N.P. Xekoukoulotakis, D. Mantzavinos, Effect of key operating parameters on phenols degradation during H₂O₂-assisted TiO₂ photocatalytic treatment of simulated and actual olive mill wastewater, *Appl. Catal. B: Environ.* 73 (2007) 11–22.
- [14] C. Cornu, J.L. Bonardet, S. Casale, A. Davidson, S. Abramson, G. Andre, F. Porcher, I. Grcic, V. Tomic, D. Vujevic, N. Koprivanac, Identification and location of iron species in Fe/SBA-15 catalysts: interest for catalytic Fenton reaction, *J. Phys. Chem. C* 116 (2012) 3437–3448.
- [15] M. Fang, T.V. Volotinen, S.K. Kulkarni, L. Belova, K.V. Rao, Effect of embedding Fe₃O₄ nanoparticles in silica spheres on the optical transmission properties of three-dimensional magnetic photonic crystals, *J. Appl. Phys.* 108 (2010) 103501–103506.
- [16] S.P. Sun, A.T. Lemley, P-nitrophenol degradation by a heterogeneous Fenton-like reaction on nano-magnetite: process optimization, kinetics, and degradation pathways, *J. Mol. Catal. A* 349 (2011) 71–79.
- [17] C.M. Cho, J.H. Noh, I. Cho, J. An, K.S. Hong, Low-temperature hydrothermal synthesis of pure BiFeO₃ nanopowders using triethanolamine and their applications as visible-light photocatalysts, *J. Am. Ceram. Soc.* 91 (2008) 3753–3755.
- [18] F. Gao, X. Chen, K. Yin, S. Dong, Z. Ren, F. Yuan, T. Yu, Z. Zou, J.M. Liu, *Adv. Mater.* 19 (2007) 2889–2892.
- [19] X.Y. Chen, T. Yu, F. Gao, H.T. Zhang, L.F. Liu, Y.M. Wang, Z.S. Li, Z.G. Zou, *Appl. Phys. Lett.* 91 (2007) 0221141–0221143.
- [20] N. Kakuta, J.M. White, A.J. Bard, A. Campion, M.A. Fox, S.E. Webber, M. Finlayson, Surface analysis of semiconductor-incorporated polymer systems. 1. Nafion and cadmium sulfide-Nafion, *J. Phys. Chem.* 89 (1985) 48–52.
- [21] G.D. Achenbach, W.J. James, R. Gerson, Preparation of single-phase polycrystalline BiFeO₃, *J. Am. Ceram. Soc.* 8 (1967) 437–438.
- [22] J.K. Kim, S.S. Kim, W.-J. Kim, Sol-gel synthesis and properties of multiferroic BiFeO₃, *Mater. Lett.* 59 (2005) 4006–4009.
- [23] C. Chen, J.R. Cheng, S.W. Yu, L. J. Che, Z.Y. Meng, Hydrothermal synthesis of perovskite bismuth ferrite crystallites, *J. Cryst. Growth* 291 (2006) 135–139.
- [24] L. Zhou, W. Wang, S. Liu, L. Zhang, H. Xu, W. Zhu, A sonochemical route to visible-light-driven high-activity BiVO₄ photocatalyst, *J. Mol. Catal. A* 252 (2006) 120–124.
- [25] N.A. Dhas, K.S. Suslick, Sonochemical preparation of hollow nanospheres and hollow nanocrystals, *J. Am. Chem. Soc.* 127 (2005) 2368–2369.
- [26] T. Soltani, M.H. Entezari, Solar photocatalytic degradation of RB5 by ferrite bismuth nanoparticles synthesized via ultrasound, *Ultrason. Sonochem.* 20 (2013) 1245–1253.
- [27] T. Soltani, M.H. Entezari, Sono-synthesis of bismuth ferrite nanoparticles with high photocatalytic activity in degradation of rhodamine B under solar light irradiation, *Chem. Eng. J.* 223 (2013) 145–154.
- [28] T. Soltani, M.H. Entezari, Photolysis and photocatalysis of methylene blue by ferrite bismuth nanoparticles under solar light irradiation, *J. Mol. Catal. A: Chem.* 377 (2013) 197–203.
- [29] J. Feng, X. Hu, P.L. Yue, H.Y. Zhu, G.Q. Lu, Discoloration and mineralization of reactive red HE-3B by heterogeneous photo-Fenton reaction, *Water Res.* 37 (2003) 3776–3784.
- [30] J. Feng, X. Hu, P.L. Yue, Novel bentonite clay-based Fe nanocomposite as a heterogeneous catalyst for photo-Fenton discoloration and mineralization of orange II, *Environ. Sci. Technol.* 38 (2004) 269–275.
- [31] P.L. Yue, J.Y. Feng, X. Hu, Photo-Fenton reaction using a nanocomposite, *Water Sci. Technol.* 49 (2004) 85–90.
- [32] J. Yu, N. Koshikawa, Y. Arai, S. Yoda, H. Saitou, Containerless solidification of oxide material using an electrostatic levitation furnace in microgravity, *J. Cryst. Growth* 231 (2001) 568–576.
- [33] M. Valant, A.-K. Axelsson, N. Alford, Peculiarities of a solid-state synthesis of multiferroic polycrystalline BiFeO₃, *Chem. Mater.* 19 (2007) 5431–5436.
- [34] T.-J. Park, G.C. Papaefthymiou, A.J. Viescas, A.R. Mooden-baugh, S.S. Wong, Size-dependent magnetic properties of single-crystalline multiferroic BiFeO₃ nanoparticles, *Nano Lett.* 7 (2007) 766–772.
- [35] D.A. Chang, P. Lin, T.Y. Tseng, Optical properties of ZrTiO₄ films grown by radio-frequency magnetron sputtering, *J. Appl. Phys.* 77 (1995) 4445–4451.
- [36] F. Mazille, T. Schoettl, N. Klammer, S. Malato, C. Pulgarin, Field solar degradation of pesticides and emerging water contaminants mediated by polymer films containing titanium and iron oxide with synergistic heterogeneous photocatalytic activity at neutral pH, *Water Res.* 44 (2010) 3029–3038.
- [37] F. Mazille, A. Lopez, C. Pulgarin, Synergistic effect of TiO₂ and iron oxide supported on fluorocarbon films. Part 2 Long-term stability and influence of reaction parameters on photoactivated degradation of pollutants, *Appl. Catal. B* 90 (2009) 321–329.
- [38] N. Murakami, T. Chiyoya, T. Tsubota, T. Ohno, Switching redox site of photocatalytic reaction on titanium (IV) oxide particles modified with transition-metal ion controlled by irradiation wave length, *Appl. Catal. A* 348 (2008) 148–152.
- [39] C.R. Keenan, D.L. Sedlak, Factors affecting the yields of oxidants from the reaction of nanoparticulate zero-valent iron and oxygen, *Environ. Sci. Technol.* 42 (2008) 1262–1267.
- [40] B. Halliwell, J.M.C. Gutteridge, Biologically relevant metal ion-dependent hydroxyl radical generation, *FEBS Lett.* 307 (1992) 108–112.
- [41] J. Fernandez, J. Bandara, A. Lopez, P. Buffar, J. Kiwi, Photoassisted Fenton degradation of nonbiodegradable azo dye (Orange II) in Fe-free solutions mediated by cation transfer membranes, *Langmuir* 15 (1999) 185–192.
- [42] F. Torrades, M. Pérez, H.D. Mansilla, J. Peral, Experimental design of Fenton and photo-Fenton reactions for the treatment of cellulose bleaching effluents, *Chemosphere* 53 (2003) 1211–1220.
- [43] N. Modirshahla, M.A. Behnajady, F. Ghanbary, Decolorization and mineralization of Cl₂ acid yellow 23 by Fenton and photo-Fenton processes, *Dyes Pigment.* 73 (2007) 305–310.
- [44] K.A. Hislop, J.R. Bolton, The photochemical generation of hydroxyl radicals in the UV-vis/ferrioxalate/H₂O₂ system, *Environ. Sci. Technol.* 33 (1999) 3119–3126.
- [45] S. Irmak, H.I. Yavuz, O. Erbatur, Degradation of 4-chloro-2-methylphenol in aqueous solution by electro-Fenton and photoelectro-Fenton processes, *Appl. Catal. B: Environ.* 63 (2006) 243–248.
- [46] R.L. Valentine, H.C.A. Wang, Iron oxide surface catalyzed oxidation of quinoline by hydrogen peroxide, *J. Environ. Eng.* 124 (1998) 31–38.
- [47] C.M. Miller, R.L. Valentine, Mechanistic studies of surface catalyzed H₂O₂ decomposition and contaminant degradation in the presence of sand, *Water Res.* 33 (1999) 2805–2816.
- [48] P.J. Vikesland, R.L. Valentine, Iron oxide surface-catalyzed oxidation of ferrous iron by monochloramine: implications of oxide type and carbonate on reactivity, *Environ. Sci. Technol.* 36 (2002) 512–519.
- [49] C.G. Hatchard, C.A. Parker, A new sensitive chemical actinometer. II. Potassium peroxyoxalate as a standard chemical actinometer, *Proc. R. Soc. Lond., Ser. A* 235 (1956) 518–536.
- [50] A.R. Khataee, M. Zarei, R. Ordikhani-Seyedlar, Heterogeneous photocatalysis of a dye solution using supported TiO₂ nanoparticles combined with homogeneous photoelectrochemical process: molecular degradation products, *J. Mol. Catal. A: Chem.* 338 (2011) 84–91.
- [51] J. Nguyen, Y. Ma, T. Luo, R.G. Bristow, D.A. Jaffray, Q.B. Lu, Direct observation of ultrafast-electron-transfer reactions unravels high effectiveness of reductive DNA damage, *Proc. Natl. Acad. Sci. USA* 108 (2011) 11778–11783.
- [52] Y. Yang, L.P. Lou, K. Wang, Y.X. Chen, Shift of initial mechanism in TiO₂-assisted photocatalytic process, *Appl. Catal. A* 301 (2006) 152–157.

- [53] W. Luo, L. Zhu, N. Wang, H. Tang, M. Cao, Y. She, Efficient removal of organic pollutants with magnetic nanoscaled BiFeO₃ as a reusable heterogeneous Fenton-like catalyst, *Environ. Sci. Technol.* 44 (2010) 1786–1791.
- [54] I. Poulios, I. Aetopoulou, Photocatalytic degradation of the textile dye reactive orange 16 in the presence of TiO₂ suspensions, *Environ. Sci. Technol.* 20 (1999) 479–487.
- [55] R.A. Burns, J.C. Crittenden, D.W. Hand, V.H. Selzer, L.L. Sutter, S.R. Salman, Effect of inorganic ions in heterogeneous photocatalysis of TCE, *J. Environ. Eng.* 125 (1999) 77–85.